Cavitation damage prediction for the JSNS mercury target vessel

Takashi Naoe[a], Hiroyuki Kogawa[a], Takashi Wakui[a], Katsuhiro Haga[a], Makoto Teshigawara[a], Hidetaka Kinoshita[a], Hiroshi Takada[a], Masatoshi Futakawa[a]

[a] *Japan Atomic Energy Agency, Tokai-mura, Naka-gun, Ibaraki 319-1195, Japan.*

Abstract

The liquid mercury target system for the Japan Spallation Neutron Source (JSNS) at the Materials and Life science experimental Facility (MLF) in the Japan Proton Accelerator Research Complex (J-PARC) is designed to produce pulsed neutrons. The mercury target vessel in this system, which is made of type 316L stainless steel, is damaged by pressure wave-induced cavitation due to proton beam bombardment. Currently, cavitation damage is considered to be the dominant factor influencing the service life of the target vessel rather than radiation damage. In this study, cavitation damage to the interior surface of the target vessel was predicted on the basis of accumulated damage data from off-beam and on-beam experiments. The predicted damage was compared with the damage observed in a used target vessel. Furthermore, the effect of injecting gas microbubbles on cavitation damage was predicted through the measurement of the acoustic vibration of the target vessel. It was shown that the predicted depth of cavitation damage is reasonably coincident with the observed results. Moreover, it was confirmed that the injection of gas microbubbles had an effect on cavitation damage.

Email address: naoe.takashi@jaea.go.jp (Takashi Naoe)

Preprint submitted to Journal of Nuclear Material (special issue on IWSMT-12) January 17, 2017

Keywords: Pressure waves, Spallation neutron source, Cavitation damage, Microbubbles, Liquid metal

---

Nomenclature

F_N : Eroded area fraction, –

N : Number of pulses, –

N_a : Acceptable number of pulses in the incubation period, –

P_N : Normalized power, –

MDE : Mean depth of erosion, μm

D_{max} : Maximum pit depth, μm

P_{bubble} : Equivalent normalized power including bubbling effect, –

V : Displacement velocity, m/s

P : Beam power, kW

Q : Peak energy deposition, J/cc/pulse

V_{bubble} : Displacement velocity with injection of gas microbubbles, m/s

t_n : Saturation time of the negative pressure, ms

a, b, c, d, e, f, and g : Constants, –

α, β, γ, δ : Constants, –

c_0, c_1, c_2 : Constants, –

ΔMDE_i : Difference of MDE, μm

MDE_i, MDE_{i-1} : MDE at the given beam condition, μm

N_i : Number of pulses at given condition, –

N'_{i-1} : Required number of pulses to reach MDE_{i-1} at the given condition i, –

P_{N_i}, $P_{N_{i-1}}$: Beam power at the given conditions of i and $i-1$, kW

MDE_{total} : Accumulated MDE, μm

D_{total} : Accumulated damage depth, μm

ε : Correction factor between off-beam and on-beam, –

1. Introduction

Liquid mercury target systems that provide pulsed neutron beams have been operated at the Japan Spallation Neutron Source (JSNS) in the Japan Proton Accelerator Research Complex (J-PARC) and the Spallation Neutron Source (SNS) at the Oak Ridge National Laboratory (ORNL) in the USA [1, 2]. High-power pulsed proton beams (the goal of the JSNS is 1 MW at a repetition rate of 25 Hz with a 1 μs pulse duration) are injected into mercury to produce spallation neutrons. Upon proton beam injection, high-amplitude pressure waves are generated by rapid heat deposition in the mercury. These pressure waves impose cyclic stresses on the enclosure vessel made of type 316L stainless steel, the so-called target vessel. The negative pressure waves caused by the difference in the sound impedance between mercury and the target vessel lead to cavitation of the mercury. This cavitation causes erosion damage of the target vessel via micro jets

and/or shockwaves generated by collapsing cavitation bubbles [3]. Such cavitation-induced damage, which is likely to increase with proton beam power and operating time, degrades the structural integrity of the target vessel and is a serious issue that may impact operational reliability under high-power operation [4]. In fact, cavitation damage with fatigue cracks was observed on the surface of the beam window of the target vessels used in the SNS [5, 6]. Cavitation damage was also observed in a target vessel in the JSNS after operating at 475 MWh for 3700 h [7].

Injection of helium gas microbubbles into mercury is one of the prospective technologies available to reduce pressure wave-induced cavitation [8]. The injected gas microbubbles absorb thermal expansion in the heating zone [9] and attenuate pressure waves using oscillating bubbles in the propagation process [10]. By numerical simulation, which was performed to calculate pressure wave propagation in mercury with homogeneously distributed gas microbubbles, the expected radius and ratio of mercury to helium gas microbubbles for mitigating pressure waves were estimated to be less than 50 μm and higher than 10^{-3}, respectively [10, 11].

A gas microbubble generator for generating bubbles of an acceptable size and desired quantity for injection into flowing mercury was installed in the mercury target system of the JSNS with a closed-loop gas supply system in October 2012 [12, 13]. Fig. 1 shows a schematic and photographs of the JSNS mercury target vessel with the gas microbubble generator. The target vessel has a triple-walled structure comprising a mercury vessel and a double-walled water-cooled shroud, a so-called safety-hull, to prevent mercury spill-out. The vessel has a reflective mirror attached to the outer surface that reflects laser beams to evalu-

ate pressure waves using a laser Doppler vibrometer, which was installed at the JSNS [14].

In this study, an empirical damage estimation procedure was proposed on the basis of cavitation damage data from off-beam experiments and on-beam experiments to predict cavitation damage to the interior surface of the mercury vessel used in the JSNS. Empirical derivation of the damage prediction procedure is described herein, and the damage predicted using this procedure is compared with observed results for a previously used mercury target to evaluate the effectiveness of injecting gas microbubbles for mitigating cavitation damage.

2. Damage prediction procedure

2.1. Cavitation damage in incubation period

It is known that the morphology of cavitation damage can be classified into roughly two stages: an incubation period and a steady state period [15, 16]. The former is the early stage of cavitation damage, where plastic deformation of the surface is dominant without noticeable mass loss. The latter is the erosion stage with significant mass loss [15]. The eroded area fraction, F_N, which is the area fraction of damage during the incubation period at a given number of pulses, is expresses as follows:

$$F_N = 1 - \exp(aN), \tag{1}$$

where a is a constant that depends on the material and testing conditions and N is the number of pulses [17]. Fig. 2 shows a typical example of the change in the eroded area fraction as a function of the number of pulses obtained from off-beam experiments in mercury using the electro-Magnetic IMpact Testing Machine (MIMTM) [18]. When the end of the incubation period is defined as $F_N = 0.98$,

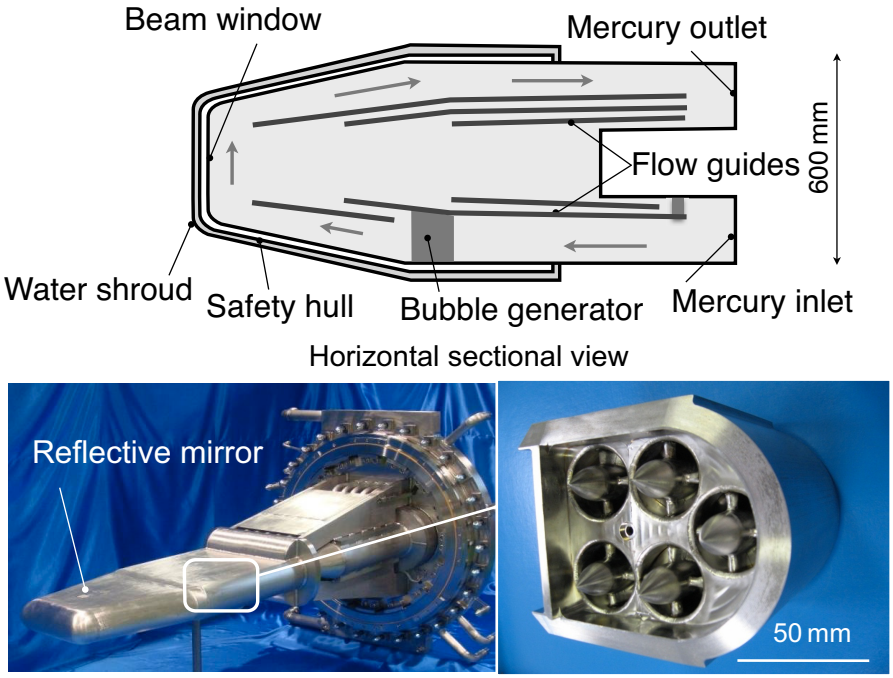

Fig. 1. Schematic and photographs of the JSNS mercury target vessel and bubble generator; multiple swirl-type bubble generators located approximately 450 mm from beam window.

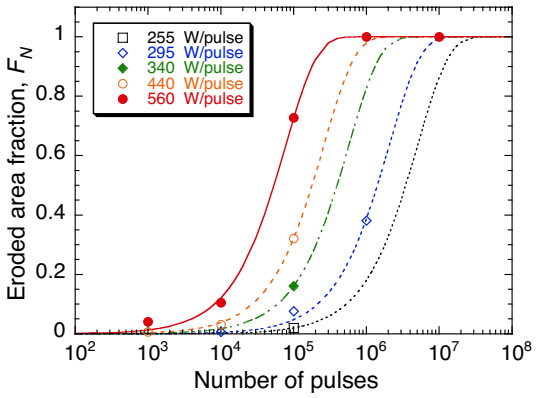

Fig. 2. Change in eroded area fraction as a function of number of pulses obtained by off-beam experiments using MIMTM.

the number of pulses in the incubation period, N_a, is estimated from Eq. (1) as follows [19]:

$$N_a = \frac{\ln 0.02}{a}. \tag{2}$$

The incubation period varies inversely and approximately with the fourth power of the normalized testing power, P_N, as follows [18]:

$$N_a = bP_N^{-c}, \tag{3}$$

where b is a constant that depends on the material and c is a constant that is empirically determined to be 3.7. Fig. 3 shows the relationship between the normalized power and the number of pulses in the incubation period obtained from off-beam (MIMTM) and on-beam experiments (WNR) [18]. WNR denotes the results of on-beam experiments using the Weapons Neutron Research at Los Alamos National Laboratory [20].

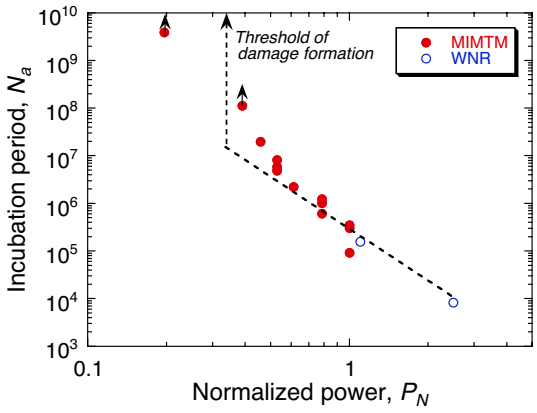

Fig. 3. Change in incubation period as a function of normalized power obtained by off-beam (MIMTM) and on-beam (WNR) experiments [18, 20].

2.2. Cavitation damage in steady state

In the steady state, cavitation erosion is usually characterized by mass loss and expressed as the Mean Depth of Erosion (*MDE*). The rate of increase of *MDE* in the steady state can be derived as a function of the number of pulses as follows [21]:

$$MDE = dN^e, \tag{4}$$

where d is a constant that depends on the incubation period, $e = 1.3$ and it is an empirically determined constant; the unit of *MDE* is μm. Fig. 4 shows the relationship between *MDE* in the steady state and the number of pulses obtained by a vibratory hone in mercury [21]. *MDE* increased at a constant rate with increasing number of pulses irrespective of the material and testing power. Assuming that *MDE* is 0.05 μm at the end of the incubation period, *MDE* can be estimated from Eqs. (3) and (4) as a functions of normalized power and number of pulses as

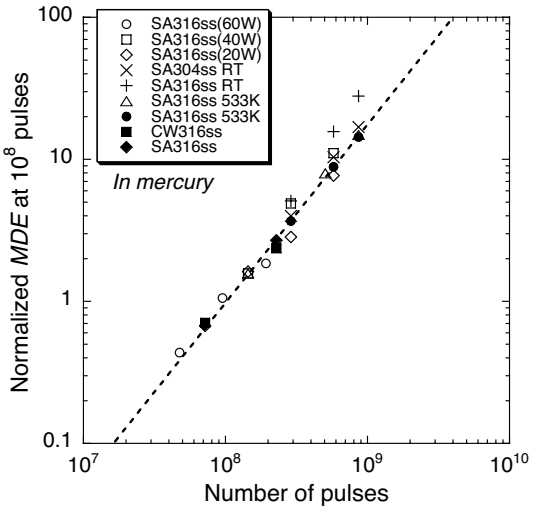

Fig. 4. Relationship between normalized MDE and number of pulses [21].

follows:

$$MDE = f(P_N^c N)^e, \tag{5}$$

where f is a constant.

2.3. Cavitation damage depth

Since MDE assumes homogeneous erosion, the lifetime and residual strength of the target vessel will be underestimated. To understand the relationship between MDE and the maximum pit depth, the pit depth distribution obtained from the MIMTM experiments were analyzed.

Fig. 5 shows the relationship between the maximum pit depth (D_{max}) and MDE as a function of the number of pulses, which was obtained from the MIMTM experiments [22]. D_{max} increased proportionally with MDE as follows:

$$D_{max} = gMDE, \tag{6}$$

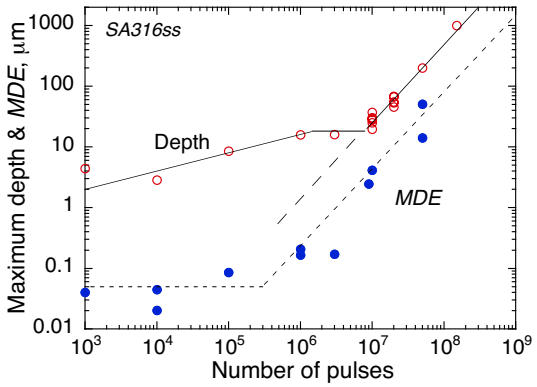

Fig. 5. Relationship among maximum pit depth, MDE, and number of pulses [22].

where g is a constant. To estimate g, the depth distribution of cavitation damage was investigated. Fig. 6 shows the probability distribution function of the pit depth for various numbers of pulses obtained in the MIMTM experiments. In particular, the depth was the average of the depth of 50 pits, which were manually selected as relatively deep pits. The scatter increased with increasing number of pulses. Fig. 7 shows the change in the ratio of the maximum pit depth to MDE as a function of the number of pulses. In particular, 99% of the Gaussian covers the obtained maximum pit depth, and the ratio of the maximum pit depth to MDE appears to be constant at pulse counts greater than 2×10^7 pulses. Therefore, g is assumed as 10 to estimate the damage depth in our cases.

2.4. Effect of injecting gas microbubbles on cavitation damage

2.4.1. Based on cavitation damage observation

Through off-beam experiments using MIMTM and in-beam experiments using WNR, it was confirmed that injecting gas microbubbles into mercury reduces cavitation damage [23, 24]. It was confirmed that cavitation damage during steady

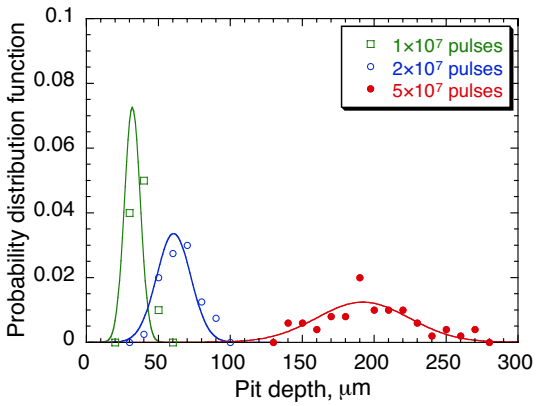

Fig. 6. Probability distribution function of pit depth for various numbers of pulses.

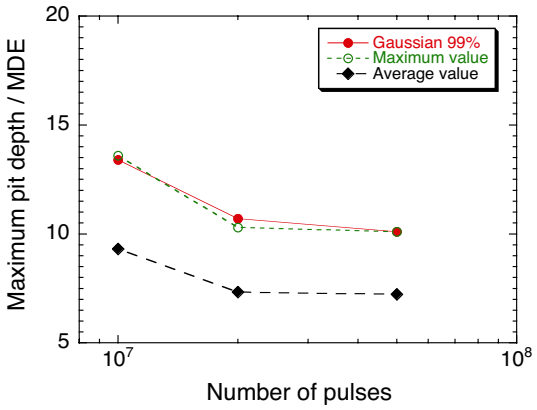

Fig. 7. Change in ratio of maximum pit depth to *MDE* as a function of number of pulses.

state follows Eq. (4) irrespective of the material and testing condition [19]. Therefore, cavitation damage under gas microbubble injection should follow Eq. (4). In this study, reduction of cavitation damage was treated as equivalent to decrease in power, i.e., the bubbling effect was considered as the scaled power. The change in the number of pulses in the incubation period with the injection of gas microbubbles was estimated as the decrease in power as follows:

$$P_{bubble} = \alpha P_N, \tag{7}$$

where α is a constant that depends on the bubbling conditions and power levels. For example, the damage area fractions in the on-beam experiment with 100 pulses of beam injection at 2.5 MW (SNS equivalent) with and without the injection of gas microbubbles were 0.09% and 0.24%, respectively [25]. On the basis of Eqs. (2) and (3), N_a and P_N of each case were estimated; then, α was estimated to be 0.78. By substituting P_{bubble} for P_N in Eqs. (5) and (6), damage depth considering the effect of injecting gas microbubbles on cavitation damage can be predicted as follows:

$$D_{max} = fg((\alpha P)_N^c N)^e. \tag{8}$$

In particular, the prediction scheme has not been experimentally verified.

2.4.2. Based on dynamic response measurement

Fig. 8 shows the time histories of the displacement velocities of the JSNS mercury target vessel obtained using a laser Doppler vibrometer (LDV) system [14, 26]. Detailed descriptions of the measurement are not given here, and it can be seen in Fig. 8 that the dynamic response (10 kHz low-pass filtered signal) from 0 to 1.5 ms dramatically decreased with the injection of gas microbubbles. It was

reported that the peak displacement velocity of the target vessel was well correlated with the proton beam conditions, including beam power and beam profile (peak energy deposition in mercury) [14]. The relationship among beam power P [kW], peak energy deposition Q [J/cc/pulse], and peak displacement velocity V [m/s] is expressed empirically as follows [14]:

$$V \approx \beta P^{\gamma} Q^{\delta}, \tag{9}$$

where β=0.011, γ=0.44, and δ=0.56 are constants obtained by the method of least squares. At the JSNS, the beam power and peak energy deposition were adjusted according to the relationship $Q = 0.011P$ for considering the balance between beam loss and pressure waves. The high-peak energy deposition (sharp beam) leads high-amplitude of pressure waves, although it is good to reduce the radiation damage and the heating of accelerator equipments, and vice versa. Therefore, the effect of gas microbubble injection on the displacement velocity of the target vessel can be expressed as a reduction of beam power as follows:

$$V_{bubble} \approx \beta P_{bubble}^{\gamma} (0.011 P_{bubble})^{\delta}, \tag{10}$$

$$P_{bubble} = \alpha P_N. \tag{11}$$

V_{bubble} at P_N = 313 kW was 0.12 m/s, as shown in Fig. 8, and α was estimated to be approximately 0.45, which was 0.78 in case of the damage observation. Hence, the effect of injecting microbubbles appears to be enhanced in comparison to that in the on-beam damage experiment.

2.5. Effect of negative pressure period on damage

It was reported that cavitation damage is correlated with beam power [18, 24]. The saturation time of negative pressure in a liquid, whose duration is proportional

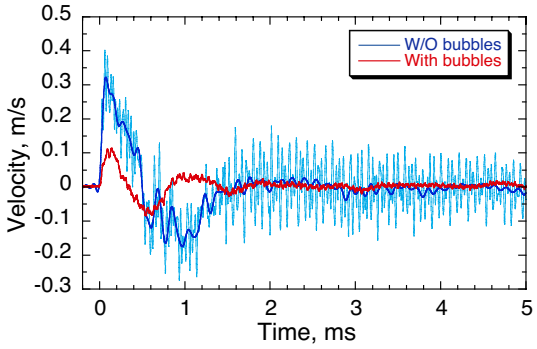

Fig. 8. Time histories of displacement velocity obtained from LDV with and without injecting gas microbubbles. Beam power and peak energy deposition of mercury in both cases ware 313 kW and 2.8 J/cc/pulse, respectively. The light blue line denotes data without microbubbles, and blue line denotes 10 kHz low-pass-filtered signal.

to the growth of the cavitation bubble and is correlated with the cavitation intensity, increases with beam power [27]. In fact, it was reported that the distribution of saturation time of the negative pressure in the SNS mercury target vessel was relatively well correlated with the distribution of cavitation damage observed on the interior surfaces [28]. In this section, the relationship between saturation time of negative pressure and beam power is explained briefly from the viewpoint of predicting damage depth based on the saturation time of negative pressure.

The numerically calculated saturation time of negative pressure at the center of the beam window portion, t_n, is expressed in terms of beam power and peak energy deposition as follows [14]:

$$t_n \approx c_0 P^{\gamma} Q^{\delta} \tag{12}$$

where c_0 is the constant for fitting, and its value is 0.054 under the JSNS target

condition. In contrast, in the off-beam experiment using MIMTM, the saturation time of negative pressure increased with power, as shown in Fig. 9, and it is expressed as follows:

$$t_n = c_1 \log P_N + c_2, \tag{13}$$

where c_1 and c_2 are constants for fitting. It is regarded that MDE is predicted as a function of the saturation time of the negative pressure using Eqs. (5), (12), and (13) as follows:

$$MDE = f(P_N^c N)^e = f((10^{\frac{c_0 P^\gamma Q^\delta - c_2}{c_1}})^c N)^e. \tag{14}$$

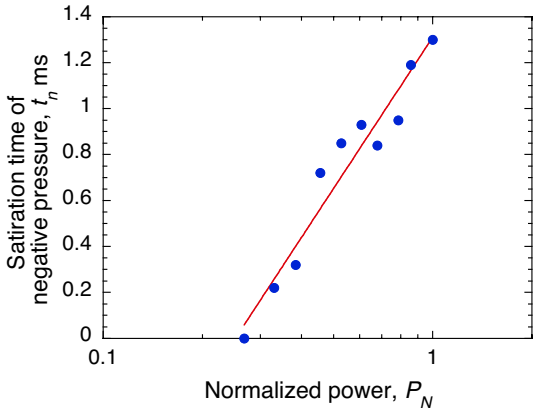

Fig. 9. Relationship between saturation time of negative pressure and normalized power obtained from off-beam experiment.

2.6. Consideration of change in beam condition

In the actual mercury target, the beam condition is not constant during operation. It is necessary to consider the effect of change in beam condition during operation. As given in Eq. (5), MDE is dependent on both power and number of pulses. Furthermore, increase in MDE within a given number of pulses at a given

constant power depends on the pre-existing MDE. Fig. 10 shows a schematic diagram of MDE under variable power. To consider the pre-existing MDE value, the increase in MDE, ΔMDE_i, at the given power, P_{N_i} and the given number of pulses, N_i, are defined as follows:

$$\Delta MDE_i = MDE_i - MDE_{i-1}, \tag{15}$$

$$= f(P^c_{N_i}(N_i + N'_{i-1}))^e - f(P^c_{N_{i-1}}N_{i-1})^e, \tag{16}$$

where N'_{i-1} is the required number of pulses in which assumes the damage MDE_{i-1} was formed at the beam condition of i expressed from Eq. (5) as follows:

$$N'_{i-1} = \frac{(MDE_{i-1}/f)^{\frac{1}{e}}}{P^c_{N_i}}. \tag{17}$$

Therefore, the accumulated MDE and the accumulated damage depth are predicted as follows:

$$MDE_{total} = \sum_{i=0}^{n} \Delta MDE_i, \tag{18}$$

$$D_{total} = gMDE_{total}. \tag{19}$$

3. Damage prediction for SNS targets

The prediction method mentioned above cannot directly predict the cavitation damage depth of the mercury target vessel because we used normalized power, P_N, defined on the basis of the off-beam experiment for predicting cavitation damage depth. That is, it is necessary to determine a correction factor to convert normalized power into proton beam power and/or intensity. To predict the damage depth to a target vessel, the correlation between P_N and beam condition was defined as a function of the peak energy deposition, Q, as follows:

$$P_N = \varepsilon \frac{Q}{17.2}, \tag{20}$$

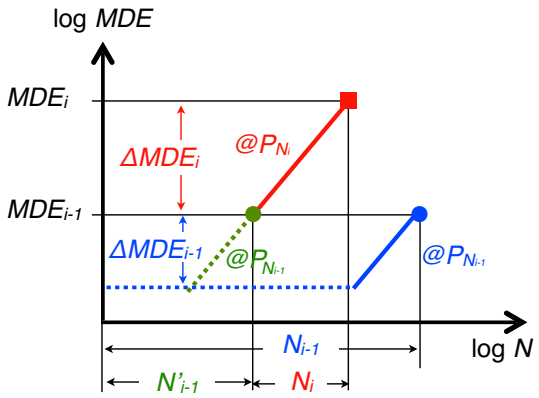

Fig. 10. Schematic illustration of MDE under the variable power.

where ε is the correction factor between the off-beam and on-beam conditions. It should be noted that the design value of the JSNS target will be Q=17.2 J/cc/pulse under 1 MW operation. Based on Eqs. (5), (18), (19), and (20), the predicted and observed damage depths of the SNS mercury target vessel were compared. It was reported that the penetration damage caused by cavitation erosion was observed on the interior surface of the first SNS target vessel [5]. The SNS target vessel has a double-walled structure at the beam window and penetration of the inner surface did not cause mercury leakage. In the case of ε=1, the predicted damage depth was only 0.4 μm, which is negligible. Thus, the correction factor was defined on the basis of damage inspection results for the SNS target vessel #1, in which cavitation damage had already penetrated the center of the inner wall at the time of replacement [5]. The correction factor, ε, was inversely estimated to be 4.09 on the assumption that the SNS target was penetrated just before replacement, hereinafter referred to as inverse estimation. Fig. 11 shows the change in the predicted damage depth of the SNS mercury target vessel as function of the operating time in the case of ε=4.09 with peak energy deposition. It is noted that the beam power

of the SNS target #1 was assumed to change from low to high. The predicted damage depth based on the saturation time of negative pressure estimated from Eqs. (14), (18), and (19), hereinafter referred to as negative pressure, is added in the Fig. 11. It can be seen that the predicted damage depth from negative pressure is deeper than the inversely predicted depth. It is considered that the relationship between the saturation time of the negative pressure period and cavitation damage might have changed in the range of the long negative pressure period caused by cavitation bubble deformation due to flow.

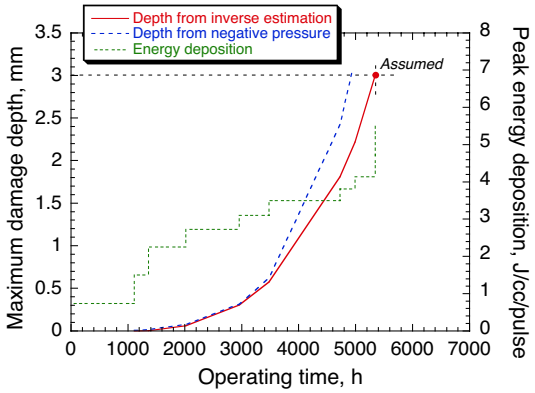

Fig. 11. Change in predicted maximum damage depth as a function of operating time. Note that the order of peak energy deposition is assumed as the descending order of low power.

4. Damage prediction for the JSNS targets

The JSNS mercury target vessel began operation in 2008, and beam power was gradually ramped up to approximately 220 kW at 25 Hz in October, 2011. The first mercury target vessel (#1) was replaced with a new mercury target vessel (#3) equipped with a microbubble generator in October 2011, and operation with

gas injection was started in October 2012. Fig. 12 shows the operational histories of the JSNS target vessels: target vessel #1 was operated from May 2008 to March 2011 and target vessel #3 was operated from December 2011 to June 2014. The accumulated beam power and operation time of the target vessels #1 and #3 are approximately 475 MWh and 3700 h, and 2050 MWh and 7500 h, respectively. The maximum accumulated dose at the beam window part was calculated as 0.67 dpa (displacement per atom) for target #1 and 2.28 dpa for target #3. In October 2014, to investigate the effect of gas microbubble injection on cavitation damage mitigation, target vessel #3 was replaced with target vessel #5, which has a double-walled structure at the beam window of the mercury vessel. It is noted that targets #2 and #4 were retained as spare targets.

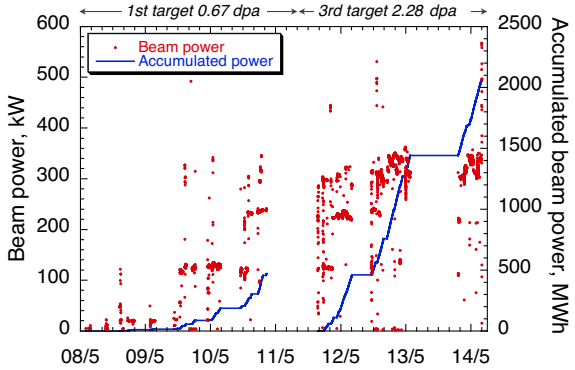

Fig. 12. Time history of operation of the JSNS mercury target vessels #1 and #3. The mercury target vessel #2 without microbubble generator was skipped for use and kept as a spare.

To confirm the validity of damage depth prediction, the predicted damage depths of the JSNS target vessel #1 through two processes based on inverse estimation and negative pressure were compared with the measured depth. Fig. 13

shows a photograph of the center part of the interior surface of the JSNS target vessel #1. A localized pit can be recognized in the damage cluster, in which pits are distributed homogeneously. The maximum depth of the localized pit was estimated to be 250 μm based on visual inspection and 3D depth profile measurement in a previous research [7]. Fig. 14 shows the change in the predicted damage depth as a function of operating time for the JSNS target vessel #1 as determined with the inverse estimation- and the negative pressure-based method. The measured damage depth falls within the range of inversely predicted values (ε=4.09). The inversely estimated value of ε using the measured damage depth was 3.91, which is slightly lower than that the value predicted using the SNS target. Overestimation of the predicted damage depth of the JSNS target based on the SNS target could be ascribed to the flow effect among other reasons because flow reduces cavitation erosion by pressure waves [23] and flow velocity around beam window of the JSNS target is higher than that of the SNS target [7]. In contrast, the measured damage depth is larger than the value predicted using the negative pressure-based method.

On the basis of the inverse estimation, the change in damage depth with gas microbubble injection for the JSNS target vessel #3 was predicted with the assumptions that α=1.0 (no effect of gas microbubbles), 0.78, 0.45 with ε=4.09, as shown in Fig. 15. The predicted damage depths based on inverse estimation were smaller than those based on negative pressure because the saturation time of negative pressure varies greatly depending on the power and location in the target at around 300 kW. It can be seen that the damage depth hardly increased under 4.0 J/cc/pulse (340 kW) in the case of α=0.45. With inverse estimation, damage depths were predicted to be 0.24 mm for α=0.45 and 0.60 mm for α=0.78 consid-

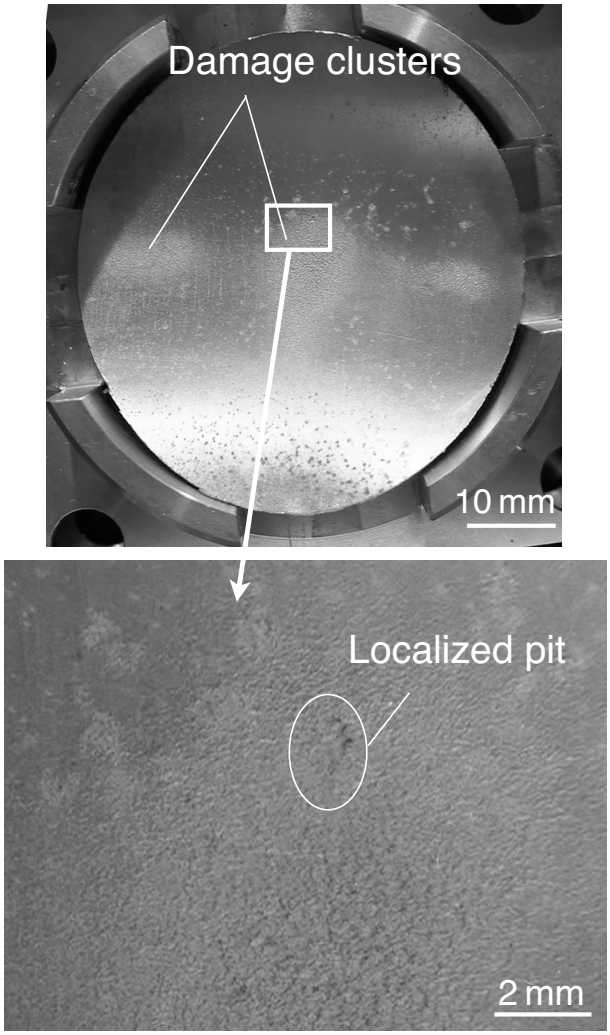

Fig. 13. Photographs of innermost disk of the JSNS mercury target vessel #1 cutout from used target vessel [7].

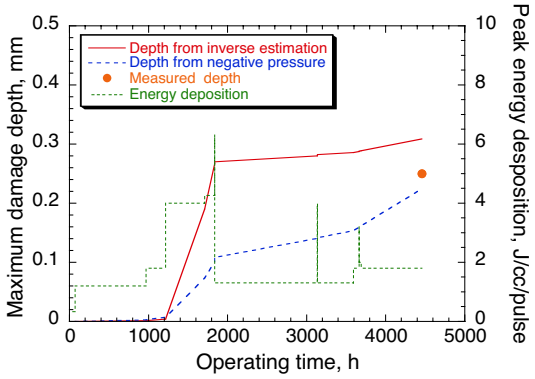

Fig. 14. Change in maximum damage depth as a function of operating time as predicted by inverse estimation and negative pressure period for the JSNS target vessel #1.

ering the bubbling effect. In contrast, damage depths predicted based on negative pressure were 0.57 mm for α=0.45 and 1.73 mm for α=0.78, respectively.

5. Damage inspection of the third JSNS target

The beam window portion of target vessel #3 was sampled after removal from service using an annular cutter to evaluate the effect of the gas microbubble injection on cavitation damage formation, and to produce specimens for post irradiation examination. The cutting was performed in a hot-cell using a remotely controlled cutting machine while the target vessel was installed on the target trolley. An annular cutter with a 55 mm outer diameter and 2.5 mm kerf was selected to sample the target. Cutting was performed without any coolant. Detailed information about the cutting and damage inspection procedures can be found in Refs. [7, 29].

Video inspection was performed using a CMOS camera to observe cavitation damage inside the interior surface of the beam window region. Since the equiva-

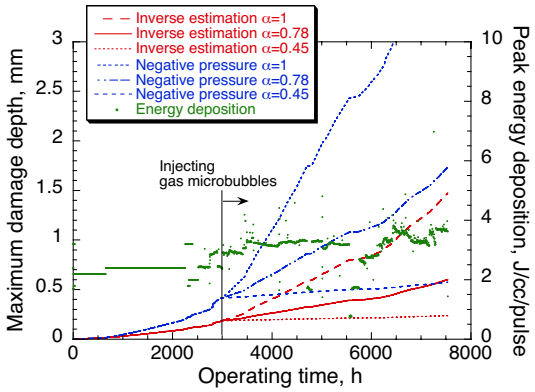

Fig. 15. Change in maximum damage depth as a function of the operating time predicted by inverse estimation and negative pressure period for the JSNS target vessel #3.

lent dose rate of the beam window was approximately 320 Sv/h, signal noise was superimposed on the images obtained using the CMOS camera. A clear image of the interior surface that demonstrated cavitation damage mitigation by gas microbubble injection was not obtained. Two of the three cameras used herein were damaged during the inspection because of high doses of radiation.

Fig. 16 shows photographs of the inner surface of the beam window and the edge of the cut hole obtained using a radiation-resistant camera. During cutting, the mercury vessel specimen fell inside the vessel. The fallen specimen was not retrieved from the target vessel because of concerns pertaining to contamination control inside the hot-cell. The visible large machining swarf suggests that the target material retained substantial ductility. Furthermore, large-scale cavitation damage was not observed unlike target vessel #1, in which the accumulated beam power was approximately 1/5 of target #3, as shown in Fig. 13. On the edge of the cut hole, severe cavitation erosion and V-shape erosion, which were observed

in the SNS target vessel [5], were not observed in the JSNS target vessel #3. In fact, cavitation damage due to proton beam-induced pressure waves was reduced by the injected gas microbubbles. Although it was impossible to quantitatively measure the damage depth of the beam window, it appears to be less than or equal to the damage depth of the target vessel #1, because a relatively smooth surface was observed on the concave inner wall surface. In the future, we will measure the damage depth of the target vessel and quantitatively evaluate the effect of microbubble injection on cavitation damage by inspecting the subsequent targets.

6. Summary

Empirical damage prediction procedures were proposed on the basis of accumulated damage data obtained from off-beam and on-beam experiments to predict cavitation damage to the mercury target vessel in the JSNS, which is considered to be the dominant factor impacting the service life of the target vessel. The effects of the injecting gas microbubbles into the mercury on the pressure wave and cavitation damage mitigation were investigated via measurement of the target surface displacement velocity and inspection of the inner wall of the used target vessel. The results showed that the damage depth can be predicted using the damage data accumulated from off-beam and on-beam experiments by following two approaches; inverse estimation of observed damage and numerical calculation of saturation time of negative pressure period. The damage depth of the JSNS target vessel #1 predicted using inverse estimation showed reasonable agreement with the damage observed in a used target vessel. Furthermore, the effect of gas microbubble injection on cavitation damage was predicted on the basis of off-beam and on-beam experiments, and compared with the visually inspected result. It

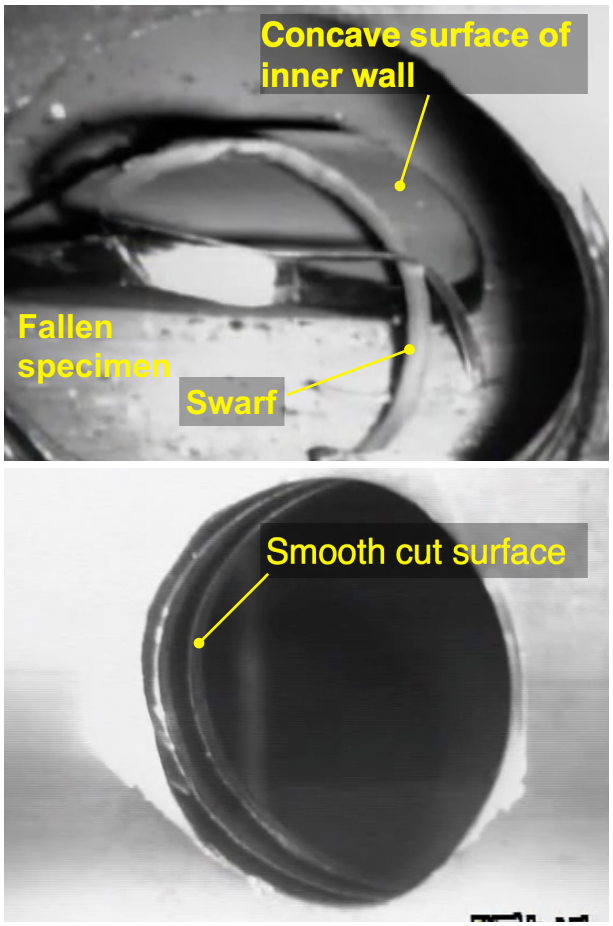

Fig. 16. Captured images of cut specimen and cut surface of target vessel #3.

was confirmed that cavitation damage is reduced by gas microbubble injection, although quantitative damage evaluation remains insufficient. In future, we will improve the precision of damage depth prediction based on the damage inspection results of subsequent targets.

Acknowledgments

The authors thank Messrs. Masakazu Seki, Hideki Ueno, Mitsunori Hirane of JAEA for their assistance with the remote handling during cutting and inspection of the target vessel. We are also indebted to Dr. Tetsuya Kai of JAEA for his help with radioactive gas control. Furthermore, we are grateful to the members of the Neutron Source Section and Radiation Safety Section of J-PARC Center for their support and advice on this work. This work was partly supported by the Japan Society for the Promotion of Science through a Grant-in-Aid for Scientific Research (23360088).

References

[1] M. Futakawa, F. Maekawa, S. Sakamoto, Neutron News 22 (2011) 15–19.

[2] T. McManamy, J. Nucl. Mater. 398 (2010) 10–14.

[3] M. Futakawa, H. Kogawa, R. Hino, H. Date, H. Takeishi, Int. J. Imact Eng. 28 (2003) 123–135.

[4] M. Futakawa, T. Naoe, H. Kogawa, M. Teshigawara, Y. Ikeda, J. Nucl. Mater. 356 (2006) 168–177.

[5] D. McClintock, B. Riemer, P. Ferguson, A. Carroll, M. Dayton, J. Nucl. Mater. 431 (2012) 147–159.

[6] B. Vevera, D. McClintock, J. Hyres, B. Riemer, J. Nucl. Mater. 450 (2014) 147–162.

[7] T. Naoe, M. Teshigawara, T. Wakui, H. Kinoshita, H. Kogawa, K. Haga, M. Futakawa, J. Nucl. Mater. 450 (2014) 123–129.

[8] K. Skala, G. S. Bauer, in: Proceedings of the meetings ICANS-XIII and ESS-PM4, Paul Scherrer Institute, Villigen, Switzerland, 1995, p. 559576.

[9] H. Kogawa, S. Ishikura, H. Sato, M. Harada, S. Takatama, M. Futakawa, K. Haga, R. Hino, S. Meigo, F. Maekawa, Y. Ikeda, J. Nucl. Mater. 343 (2005) 178–183.

[10] K. Okita, S. Takagi, Y. Matsumoto, J. Fluid Sci. Technol. 3 (2008) 116–128.

[11] M. Futakawa, H. Kogawa, S. Hasegawa, T. Naoe, M. Ida, K. Haga, T. Wakui, N. Tanaka, Y. Matsumoto, Y. Ikeda, J. Nucl. Sci. and Technol. 45 (2008) 1041–1048.

[12] H. Kogawa, K. Haga, T. Naoe, H. Kinoshita, M. Ida, M. Futakawa, in: Proceedings of the meetings ICANS-XIX, Paul Scherrer Institute, Villigen, Switzerland, 2010, pp. CD–ROM.

[13] H. Kogawa, M. Futakawa, T. Naoe, M. Harada, K. Haga, T. Wakui, J. Nucl. Sci. and Technol. (2015) In press.

[14] H. Kogawa, T. Naoe, H. Kyotoh, K. Haga, H. Kinoshita, M. Futakawa, J. Nucl. Sci. Technol. under reviewing (2015).

[15] ASTM G32-92, ASTM International, West Conshohocken, PA, 1992.

[16] H. Mori, S. Hattor, T. Okadai, JSME Int. J. A41 (1998) 96–102.

[17] H. Soyama, M. Futakawa, K. Homma, J. Nucl. Mater. 343 (2005) 116–122.

[18] M. Futakawa, T. Naoe, H. Kogawa, Y. Ikeda, J. Nucl. Sci. Technol. 41 (2004) 1059–1064.

[19] M. Futakawa, T. Naoe, C. C. Tsai, H. Kogawa, S. Ishikura, Y. Ikea, H. Soyama, H. Date, J. Nucl. Mater. 343 (2005) 70–80.

[20] J. R. Haines, B. W. Riemer, D. K. Felde, J. D. Hunn, S. J. Pawel, C. C. Tsai, J. Nucl. Mater. 343 (2005) 58–69.

[21] M. Futakawa, T. Naoe, H. Kogawa, C. C. Tsai, Y. Ikeda, J. Nucl. Sci. and Technol. 40 (2003) 895–904.

[22] T. Naoe, M. Futakawa, T. Ooi, T. Wakui, Y. Motohashi, J. Soc. Mater. Sci. Japan 55 (2006) 944–950. In Japanese.

[23] T. Naoe, M. Futakawa, M. Ida, Nucl. Inst. Meth. in Phys. Res. A 586 (2008) 382–386.

[24] B. Riemer, J. Haines, M. Wendel, G. Bauer, M. Futakawa, S. Hasegawa, H. Kogawa, J. Nucl. Mater. 377 (2008) 162–173.

[25] B. Riemer, M. Wendel, D. Felde, R. Sangrey, A. Abdou, D. West, T. Shea, S. Hasegawa, H. Kogawa, T. Naoe, C. Farny, A. Kaminsky, Journal of Nuclear Materials 450 (2014) 192–203.

[26] M. Teshigawara, T. Wakui, T. Naoe, H. Kogawa, F. Maekawa, M. Futakawa, K. Kikuchi, J. Nucl. Mater. 398 (2010) 283–243.

[27] M. Futakawa, T. Naoe, H. Kogawa, K. Haga, K. Okita, Exp. Therm. Fluid Sci. 57 (2014) 365–370.

[28] B. Riemer, D. McClintock, S. Kaminskas, A. Abdou, J. Nucl. Mater. 450 (2014) 183–191.

[29] H. Kinoshita, K. Haga, M. Seki, T. Suzuki, M. Ito, Y. Kasugai, T. Wakui, K. Kogawa, T. Naoe, K. Hanano, M. Teshigawara, F. Maekawa, S. Nakamoto, M. Futakawa, in: Proceedings of the meetings ICANS-XX, Commission Nacional de Energia Atomica, 2012, p. 334.